Improving supersonic flights with femtosecond laser filamentation

Paul-Quentin Elias, Nicolas Severac, Jean-Marc Luyssen, Yves-Bernard André, Ivan Doudet, Benoît Wattellier, Jean-Pierre Tobeli, Sylvain Albert, B. Mahieu, Reynald Bur, et al.

APPLIED SCIENCES AND ENGINEERING

Improving supersonic flights with femtosecond laser filamentation

P.-Q. Elias[1]*, N. Severac[2], J.-M. Luyssen[2], Y.-B. André[3], I. Doudet[4], B. Wattellier[4], J.-P. Tobeli[2], S. Albert[3], B. Mahieu[3], R. Bur[2], A. Mysyrowicz[3], A. Houard[3]

When a flying object becomes supersonic, a concomitant increase in drag leads to a considerable rise in fuel consumption. We show experimentally that an embarked terawatt femtosecond laser can significantly decrease this drag. We measured a 50% transient reduction of drag on a test model placed in a supersonic wind tunnel at Mach 3. This effect was initiated by the thin hot air column created in front of the supersonic object by filamentation of the laser pulse. We also show that this technique offers possibilities for steering.

INTRODUCTION

When a body moves in the atmosphere with a velocity V_∞ exceeding the sound velocity c_0, a shock wave is generated. This leads to a considerable increase in the drag experienced by the supersonic object towing the shock wave (*1*). This shock wave increases fuel consumption and produces a sonic boom that renders regular supersonic flight above populated area unacceptable. A common strategy to mitigate these nefarious effects is to give a long and slender shape to the body in the form of a spike. This results in a gradual deviation of the flow with a weaker oblique shock and sonic boom.

However, there are limits imposed on the aspect ratio of the spike, either because of structural constraints (vibrations and mechanical stress) or constraints related to maneuverability. Several authors have suggested that an immaterial spike in the form of a long plasma column would help circumvent these limits (*2*–*4*). The plasma filaments formed by ultrashort laser pulses are particularly attractive for this purpose because of their ability to produce linear energy deposition over distances ranging from centimeters to meters (*5*–*8*). Even the small disturbance created by a weightless laser-induced spike should lead to a substantial improvement of the drag coefficient of the flying object without affecting otherwise its flying performances. It could also be used to provide a steering mechanism with no moving mechanical parts. However, the actual demonstration of this phenomenon is still lacking.

We have successfully reduced by half the instantaneous drag experienced by a test model placed in a Mach 3 supersonic wind tunnel. This is achieved by an intense ultrashort infrared laser pulse emerging from the front of the model. The converging laser pulse deposits part of its energy upstream along a thin filamentary plasma column (*9*, *10*). Convection pushes the subsequent hot air disturbance to the front of the test model, where its expansive cooling leads to a depression responsible for the reduction of drag. Hydrodynamic simulations show that the average drag reduction with a laser operating at multiple kilohertz repetition rate could amount to 10 to 20%.

MATERIALS AND METHODS

The principle of the experiment is the following (more details about the experimental set up are found in the supplementary materials). A test model was inserted in a Mach 3 supersonic wind tunnel. It was a blunted cone, 60 mm in diameter, mounted on a balance equipped with three high-stiffness strain gauges to measure the axial component of the drag. Two piezoelectric pressure transducers were also mounted on the sides of the test model to record the pressure fluctuations on the upper and lower parts of the model.

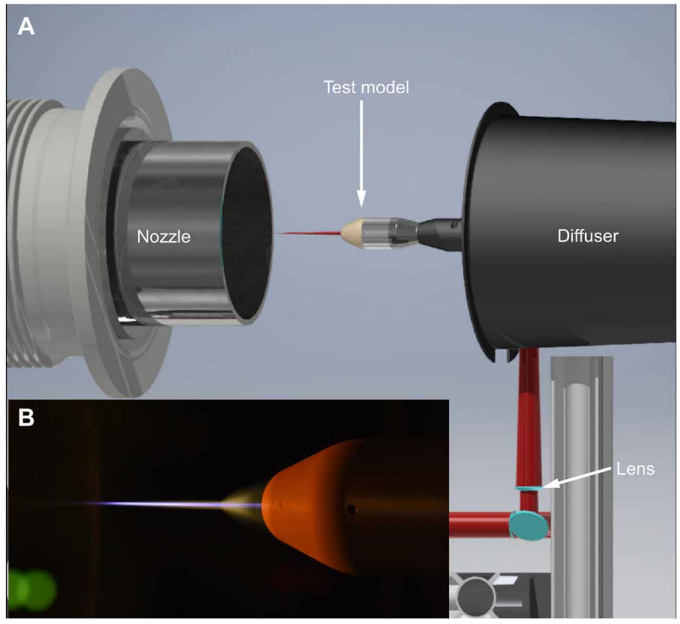

Fig. 1. Experimental Arrangement. (**A**) Computer-assisted drawing view of the experimental setup. The supersonic air flow emerges from the left. The test model is located 160-mm downstream of the nozzle exit section. The laser beam (shown in dark red) is steered from below by mirrors toward the test model from where it emerges toward the left. It is focused by a converging lens (focal length, 1000 mm), with its focal point 50-mm upstream of the model nose. Side windows on the test section provide an optical access to the test model in the flow. (**B**) Photograph of the test model in the presence of the femtosecond laser pulse in an $M = 3$ supersonic flow. White and violet correspond to the broadband continuum and plasma luminescence from the filament, respectively. The conical emission near the front nose is due to the plasma emission in the recirculating bubble. Photo credit: Aurélien Houard, LOA-CNRS.

[1]DPHY, ONERA, Université Paris Saclay, F-91123 Palaiseau, France. [2]DAAA, ONERA, Université Paris Saclay, F-92190 Meudon, France. [3]Laboratoire d'Optique Appliquée, ENSTA ParisTech, CNRS, Ecole Polytechnique, Palaiseau F-91762, France. [4]Phasics, Espace technologique, route de l'Orme des Merisiers, F-91190 Saint-Aubin, France.
*Corresponding author. Email: paul-quentin.elias@onera.fr

The comparison between the top and bottom pressure signals also provides information about the pressure asymmetry with respect to a vertical plane (see Fig. 1A). A femtosecond laser pulse from a mobile terawatt laser was guided in the test model body and emerges from the nose of the object at the stagnation point location through a 3-mm hole. The beam was focused into the flowing air, with a focal point located about 50-mm upstream of the body. In view of its terawatt peak power, the propagating laser pulse assumes a narrow and intense filamentary beam waist around the geometrical focus of the laser beam (see Fig. 1B). The peak laser intensity in the filament region was sufficiently high to ionize air molecules. The deposited laser energy led to the sudden creation of a short-lived plasma column and to the subsequent development of a shock wave that expanded laterally, leaving behind a long-lived hot and thin neutral air channel of reduced density (*11*, *12*). A wavefront sensor [Phasics SID4 HR (*13*)] provided the sign and magnitude of the filamentation-induced changes of neutral air density in the low-density channel and in the lateral shock wave at various times after the laser pulse. These variations were used to compute the energy deposited in the flow by the laser filament (see the supplementary materials).

A second collimated nanosecond laser pulse propagating perpendicular to the air flow axis was used for imaging the low-density

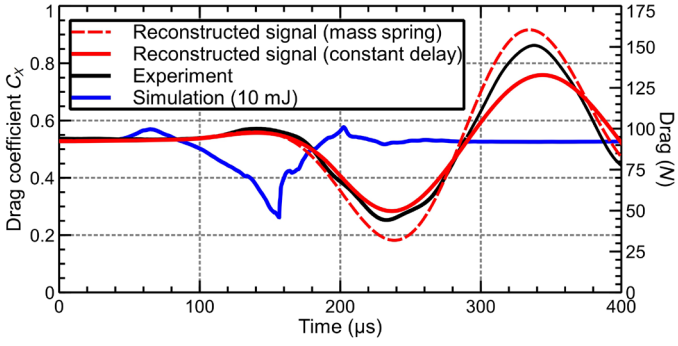

Fig. 2. Experimental drag signal measured by the balance (in black) and drag computed from the simulation for a deposited energy of 10 mJ (in blue). The laser pulse is at $t = 0$. The corresponding energy of the 50-fs laser pulse emerging from the front nose is 100 mJ. The red curves show the reconstructed drag signal obtained by convoluting the computed drag signal with estimates of the balance transfer function (damped second-order system) by adding either a constant delay (continuous line) or a secondary spring-mass system (dashed line) to account for the model nose deformation (see the supplementary materials).

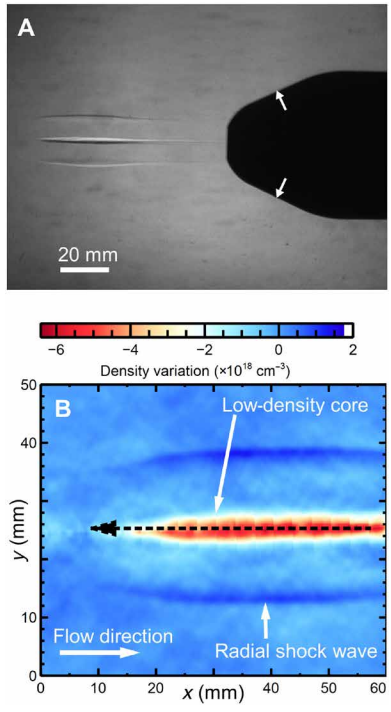

Fig. 3. Formation of a low-density core by the laser energy deposition. (**A**) Schlieren image in static air recorded 17.2 μs after the laser pulse, showing the central low-density core and the lateral shock wave. The location of the pressure sensors is shown by the two white arrows. (**B**) Density variations induced by the laser filament during a test run, 40.3 μs after the laser pulse. The variations are given relative to the stream number density $n_0 = 6.4 \times 10^{18}$cm^{-3} in the absence of laser.

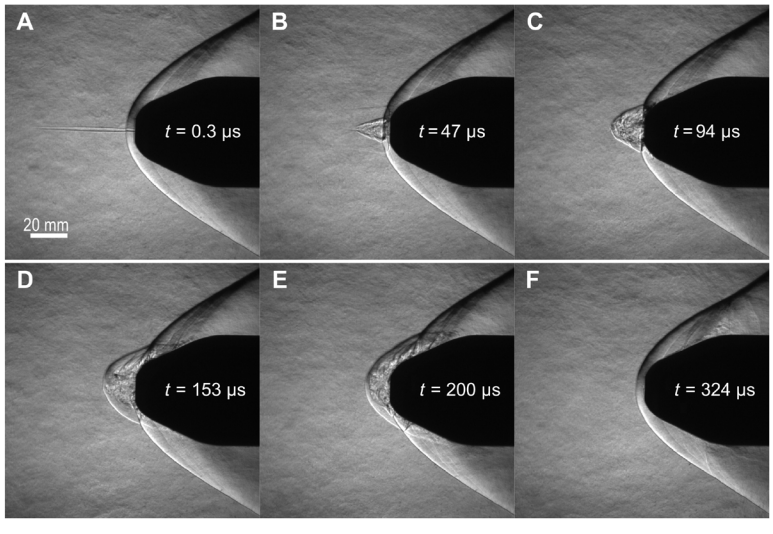

Fig. 4. Interaction of the laser energy deposition with the supersonic flow. Time-resolved schlieren images in the presence of Mach 3 air flow coming from the left, recorded at different delays after the laser shot: 0.3 μs (**A**), 47 μs (**B**), 94 μs (**C**), 153 μs (**D**), 200 μs (**E**), and 324 μs (**F**). The formation of a bubble upstream of the front nose is followed by a downstream expansion flow along the test model surface and the recovery of initial conditions after 300 μs.

column, the lateral shock wave, and the supersonic shock wave surrounding the body by the schlieren technique. Briefly, any irregularities in the air refractive index, such as reduced or increased air density zones, diffract the collimated laser beam. By collecting the diffracted rays of the nanosecond laser pulse as a function of its delay with respect to the femtosecond laser pulse, one obtains nanosecond time-resolved images of the shock waves and of the evolving low-density canal.

RESULTS AND DISCUSSION

A notable signal is measured by the balance in response to a laser pulse (see Fig. 2). The comparison of the sign of the signal with that obtained from calibrated percussion of the test model nose shows that there is a transient reduction of drag induced by the laser pulse (see the supplementary materials for the procedure). However, because of its limited bandwidth, the balance acts as a filter for the true drag, which leads to a delay of its response, as seen in Fig. 2. From this filtered drag signal, however, one can compute the mechanical impulse imparted to the test model. The true time evolution of the drag is retrieved by comparison between experimental results and simulations (as shown below).

Schlieren images recorded at different delays from the femtosecond laser pulse allow understanding the origin of the drag reduction. Figure 3 shows the neutral air density measured by the wavefront sensor and the schlieren image of the flow field around the body

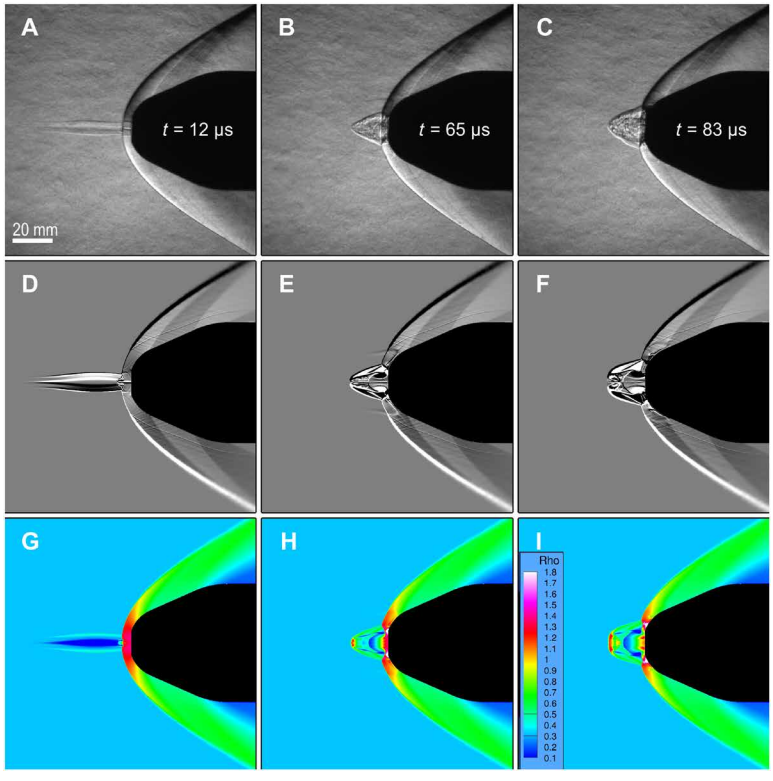

Fig. 5. Comparison of experimental and numerical results. Schlieren image of the shock wave disturbance obtained 12 µs (**A**), 65 µs (**B**), and 83 µs (**C**) after the laser pulse. The corresponding numerical schlieren images obtained from the numerical simulation are respectively shown in (**D**), (**E**), and (**F**), and the calculated gas density field is shown in (**G**), (**H**), and (**I**).

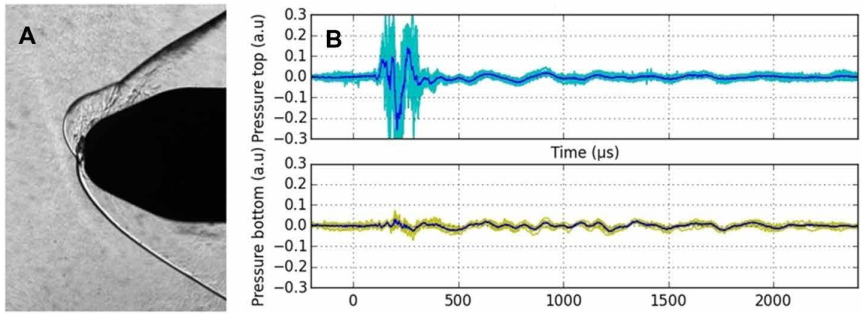

Fig. 6. Effect of an off-axis energy deposition. (**A**) Image of the shock wave disturbance obtained after 200 µs by a laser propagating slightly off axis. Since the shock front in the upper part of the figure is detached from the object surface, it leads to a net asymmetric drag that steers the object upward. (**B**) Corresponding signal from the piezoelectric pressure gauges in arbitrary units (a.u). The two pressure gauges are mounted vertically in a plane centered on the model axis, as shown in Fig. 3. The upper and lower curves of the figure show the signals detected by the corresponding gauges. Only the upper lying gauge responds significantly, indicating an upward directed decrease in drag.

with the laser in the absence of air flow. In this image, recorded 6.2 μs after the laser shot, one can observe a 10-cm-long central hot channel of low air density generated by the filament and a radially expanding shock front, more apparent in movies S1 and S2. In the presence of air flow, the hot channel is convected toward the test model front nose where it interacts with the detached bow shock. The simulation shows that the combination of the radial density gradient of the hot channel with the axial pressure gradient of the shock front induces a baroclinic torque that produces vorticity (*14*) and induces a forward-propagation recirculating bubble. During this phase, the pressure at the model nose front rises, and the drag signal shows a small increase, as shown in Fig 2. This transient increase is due to the interaction of the conical shock formed by the expanding recirculating bubble and the detached shock of the blunt body. This interaction deflects the incoming flow inward, resulting in a high-pressure jet impinging on the front nose. When the hot channel is entirely convected in the recirculating zone, the forward propagation ceases. The recirculating flow forms a toroidal vortex that expands radially and then progressively flows downstream along the test body surface (Fig. 4). As can be seen in Fig. 5, these schlieren images are well restituted by the hydrodynamic code CEDRE from ONERA, where the measured deposited laser energy and the air flow conditions are taken as input conditions (*15*). The lower pressure at the core of the vortex is at the origin of the drag reduction. It corresponds to a peak reduction of drag amounting to more than 50% when the deposited laser energy reaches 10 mJ (see Fig. 2). The quantity of absorbed laser energy is obtained from absolute measurements of density in the heated air channel.

We have also performed measurement with a slight misalignment of the laser direction with respect to the blunt body axis. It results in an asymmetric disturbance of the shock wave (see Fig. 6) that can act as a mechanism for guidance. Since the shock front becomes more detached from the object surface in the upper part of the figure, it leads to a net asymmetric drag that steers the object upward, a fact confirmed by the different responses of the vertically mounted piezoelectric pressure gauges.

PERSPECTIVES

This experiment is meant as a proof-of-principle demonstration. The experiment was carried out with a laser of low repetition rate (10 Hz). Since the flow disturbance dies after 300 μs, the average change of drag is insignificant. In addition, the weight of the laser (~1.2 tons) is prohibitive. Is the idea of an embarked laser in a supersonic vehicle nevertheless reasonable? We note that rapid progress is being made in the technology of all solid, diode-pumped terawatt laser systems operating at a repetition rate of multiple kilohertz (*16*). Filamentation in air over distances reaching several meters has been demonstrated recently with a kilohertz terawatt laser prototype (*17*). Prototypes operating at several kilohertz are under development. Our simulations show that a 10-kHz terawatt laser with a filament length similar to that of our experiment should reduce the average drag by 10 to 20% for a Mach 3 speed. Increasing the filament length would further improve the efficiency of the immaterial spike (*6*). Diode-pumped lasers have good overall efficiency, and their weight can be substantially reduced since the vital components of the laser (diodes, gratings, mirrors, and amplifying films) are light, while accessories such as power supply and cooling could be derived from the flying vehicle. In addition, we reiterate that slightly deviating the beam direction from the vehicle axis presents a possible means of weightless steering. We therefore believe that a supersonic vehicle equipped with a laser spike is in the realm of future possibilities.

SUPPLEMENTARY MATERIALS

Supplementary material for this article is available at http://advances.sciencemag.org/cgi/content/full/4/11/eaau5239/DC1

Section S1. Experimental setup
Section S2. Characteristics of the femtosecond laser
Section S3. Details of the test model
Section S4. Extraction of the change of drag induced by the laser pulse
Section S5. Wavefront sensor device to measure the filament induced changes of air density
Section S6. Simulations
Fig. S1. General view of the experimental setup.
Fig. S2. Response of the strain gauge to a femtosecond laser pulse and to a percussion shock from a falling sphere.
Movie S1. Schlieren images showing the time evolution of the laser energy deposition in the Mach 3 flow.
Movie S2. Schlieren images showing the time evolution of the laser energy deposition in quiescent air at atmospheric pressure.

REFERENCES AND NOTES

1. J. Anderson Jr., *Fundamentals of Aerodynamics* (McGraw-Hill, ed. 3, 1985).
2. Y. F. Kolesnichenko, V. G. Brovkin, S. B. Leonov, A. A. Krylov, V. A. Lashkov, I. C. Mashek, A. A. Gorynya, M. I. Ryvkia, Investigation of AD-Body Interaction with Microwave Discharge Region in Supersonic Flows, in *39th Aerospace Sciences Meeting and Exhibit* AIAA-2001-0345, Reno, NV, 8 to 11 January 2001.
3. Y. F. Kolesnichenko, O. A. Azarova, V. F. Brovkin, D. V. Khmara, V. A. Lashkov, I. C. Mashek, M. I. Ryvkin, Basics in Beamed MW Energy Deposition for Flow / Flight Control, in *42nd AIAA Aerospace Sciences Meeting and Exhibit* AIAA-2004–669, Reno, Nevada, 5 to 8 January 2004.
4. D. Knight, Y. F. Kolesnichenko, V. Brovkin, D. Khmara, V. Lashkov, I. Mashek, Interaction of a microwave-generated plasma with flow past a hemisphere cylinder at Mach 2.1. *AIAA J.* **47**, 2996–3010 (2009).
5. K. Kremeyer, K. A. Sebastian, C.-W. Shu, Computational study of shock mitigation and drag reduction by pulsed energy lines. *AIAA J.* **44**, 1720–1731 (2006).
6. P.-Q. Elias, Numerical simulations on the effect and efficiency of long linear energy deposition ahead of a supersonic blunt body : Toward a laser spike. *Aerosp. Lab J.* 1–11 (2015).
7. M. Golbabaei-Asl, D. D. Knight, Numerical characterization of high-temperature filament interaction with blunt cylinder at Mach 3. *Shock Waves* **24**, 123–138 (2013).
8. L. A. Johnson, P. Sprangle, Guiding supersonic projectiles using optically generated air density channels. *J. Appl. Phys.* **118**, 123301 (2015).
9. A. Couairon, A. Mysyrowicz, Femtosecond filamentation in transparent media. *Phys. Rep.* **441**, 47–189 (2007).
10. G. Point, Y. Brelet, A. Houard, V. Jukna, C. Milián, J. Carbonnel, Y. Liu, A. Couairon, A. Mysyrowicz, Superfilamentation in air. *Phys. Rev. Lett.* **112**, 223902 (2014).
11. Y.-H. Cheng, J. K. Wahlstrand, N. Jhajj, H. M. Milchberg, The effect of long timescale gas dynamics on femtosecond filamentation. *Opt. Express* **21**, 4740–4751 (2013).
12. G. Point, E. Thouin, A. Mysyrowicz, A. Houard, Energy deposition from focused terawatt laser pulses in air undergoing multifilamentation. *Opt. Express* **24**, 6271–6282 (2016).
13. G. R. Plateau, N. H. Matlis, C. G. Geddes, A. J. Gonsalves, S. Shiraishi, C. Lin, R. A. van Mourik, W. P. Leemans, Wavefront-sensor-based electron density measurements for laser-plasma accelerators. *Rev. Sci. Instrum.* **81**, 033108 (2010).
14. A. A. Zheltovodov, E. A. Pimonov, Numerical simulation of an energy deposition zone in quiescent air and in a supersonic flow under the conditions of interaction with a normal shock. *Tech. Phys.* **58**, 170–184 (2013).
15. A. Refloch, B. Courbet, A. Murrone, P. Villedieu, C. Laurent, P. Gilbank, J. Troyes, L. Tessé, G. Chaineray, J. B. Dargaud, E. Quémerais, F. Vuillot, CEDRE Software. *J. AerospaceLab* 1–10 (2011).
16. H. Fattahi, H. G. Barros, M. Gorjan, T. Nubbemeyer, B. Alsaif, C. Y. Teisset, M. Schultze, S. Prinz, M. Haefner, M. Ueffing, A. Alismail, L. Vámos, A. Schwarz, O. Pronin, J. Brons, X. Tao Geng, G. Arisholm, M. Ciappina, V. S. Yakovlev, D.-E. Kim, A. M. Azzeer, N. Karpowicz, D. Sutter, Z. Major, T. Metzger, F. Krausz, Third-generation femtosecond technology. *Optica* **1**, 45–63 (2014).
17. A. Houard, V. Jukna, G. Point, Y. B. André, S. Klingebiel, M. Schultze, K. Michel, T. Metzger, A. Mysyrowicz, Study of filamentation with a high power high repetition rate ps laser at 103 μm. *Opt. Express* **24**, 7437–7448 (2016).

Acknowledgments: We acknowledge the technical support received during the experiments from F. Lambert and J. Carbonnel. **Funding:** This project received funding from DGA though contract ANR ASTRID no. ANR-15-00008-001. **Authors contributions:** P.-Q.E., A.H., A.M., and R.B. designed the experiment. J.-P.T., R.B., P.-Q.E., and A.H. designed the test model. J.-P.T. designed the test balance. I.D. and B.W. performed the wavefront sensor measurements. P.-Q.E. performed the schlieren measurements. N.S. and J.M.L. ran the wind tunnel experiments. A.H., B.M., S.A., and Y.-B.A. operated and tuned the femtosecond laser. P.-Q.E. performed the simulation. A.M., A.H., and P.-Q.E. wrote the manuscript with inputs from the other authors. **Competing interests:** The authors declare that they have no competing interests. **Data and materials availability:** All data needed to evaluate the conclusions in the paper are present in the paper and/or the Supplementary Materials. Additional data related to this paper may be requested from the authors. The experimental data related to the wind tunnel tests can be provided by ONERA pending scientific review and a completed material transfer agreement. Requests for these data should be submitted to ONERA.

Submitted 19 June 2018
Accepted 27 September 2018
Published 2 November 2018
10.1126/sciadv.aau5239

Citation: P.-Q. Elias, N. Severac, J.-M. Luyssen, Y.-B. André, I. Doudet, B. Wattellier, J.-P. Tobeli, S. Albert, B. Mahieu, R. Bur, A. Mysyrowicz, A. Houard, Improving supersonic flights with femtosecond laser filamentation. *Sci. Adv.* **4**, eaau5239 (2018).

Science Advances

Improving supersonic flights with femtosecond laser filamentation

P.-Q. Elias, N. Severac, J.-M. Luyssen, Y.-B. André, I. Doudet, B. Wattellier, J.-P. Tobeli, S. Albert, B. Mahieu, R. Bur, A. Mysyrowicz and A. Houard

Sci Adv **4** (11), eaau5239.
DOI: 10.1126/sciadv.aau5239